Polaron-enhanced giant strain effect on defect formation: The case of oxygen vacancies in rutile TiO_2

Yi-Feng Zheng,[1,2] Shiyou Chen,[3] Ji-Hui Yang,[1] and Xin-Gao Gong[1,2]

[1]*Department of Physics, Key Laboratory for Computational Science (MOE), State Key Laboratory of Surface Physics, Fudan University, Shanghai 200433, China*

[2]*Collaborative Innovation Center of Advanced Microstructures, Nanjing 210093, Jiangsu, China*

[3]*Key Laboratory of Polar Materials and Devices (MOE), East China Normal University, Shanghai 200241, China*

(Received 12 October 2018; published 25 January 2019)

Recently, a semiconductor-to-metal transition was surprisingly observed in rutile TiO_2 by applying just 5% tensile strain. To explore the mechanism behind this giant strain effect, we performed first-principles calculations focusing on the commonly existing oxygen vacancies (OVs) in rutile TiO_2. We find that 5% biaxial tensile strain largely reduces the formation energies of OVs and biaxial compressive strain increases the formation energies of OVs. While our findings are in agreement with experiments, the giant strain effects on OV defect formation energies cannot be well explained by, or may even contradict, the common continuum elastic model. Our further studies show that strain not only induces elastic energy gain during defect formation, but also changes the polaronic configurations, which can have either energy gain or loss depending on the occupations of the excess electrons. The large reduction of OV formation energy under tensile strain is thus a combined effect of both elastic and polaronic energy gain. This giant strain effect, enhanced by polaronic effects on defect formation, might provide an alternative method for the manipulation of defects and electric conductivity in rutile TiO_2 and other semiconducting materials.

DOI: 10.1103/PhysRevB.99.014113

I. INTRODUCTION

Strain has been widely used to tune the properties of various materials, with one intensively explored area being the interplay between strain and defect properties. For instance, strain can be used to enhance doping solubility in semiconductors [1], to lower the formation energy of oxygen vacancies (OVs), and induce an ordered phase in epitaxial strained $La_{0.5}Sr_{0.5}CoO_{3-\delta}$ film [2]. Tensile strain in thin films of perovskite-based $SrCoO_x$ created more OVs and enhanced cobaltite's catalytic activity towards the oxygen evolution reaction [3,4]. Strain also influenced the diffusion properties of defects such as interstitial Mn in GaAs [5] or OVs in bulk and subsurface rutile TiO_2 [6]. Usually, strain effects on defect formations are described by the continuum elastic model, which assumes that the stress is proportional to the strain and the potential energy is parabolic with the strain. This model has been used to successfully explain the monotonic change of impurity formation energy with strain [1] and parabolic behavior of OV formation energy with strain [2]. However, when the occupation of electronic energy levels changes significantly under strain, the continuum elastic model might fail [7].

TiO_2 is a prototypical metal oxide applicable in wide-ranging areas. It can be used for electrochemical photolysis of water [8] and assist in catalyzing the oxidation of carbon monoxide [9]. The defect physics of OVs in rutile TiO_2 was studied extensively both in experiments [10–12] and by first-principles calculations [13–15], with a majority of interest in the OVs on the TiO_2 (110) surface. Other defects, such as Ti interstitials [16,17] and hydroxyl groups [13] also attracted considerable research interest. It is generally believed that excess electrons tend to localize at Ti sites and are responsible for the band-gap states observed in experiments [11,18]. Strain has been used to modulate defect properties in TiO_2. First-principles calculations indicated that the formation energies of different types of OVs in strained TiO_2 (110) depended on the external strain and the distributions of OVs could thus be engineered [19]. Recent experiments have reported a semiconductor-to-metal transition in rutile TiO_2 induced by tensile strain [20]. They proposed that strain raised the energy distribution of OVs while a large amount of new OVs created by strain was unlikely. However, this is different from theoretical findings. It has been found [19] that tensile strain can decrease the formation energies of OVs on the (110) surface of rutile TiO_2 and thus the OV concentration can be increased. Whether the OV concentration increases under tensile strain and how it is related to the semiconductor-to-metal transition remain controversial and require further explorations of strain effects on OV formations to understand the semiconductor-to-metal transition in TiO_2.

While one can take it for granted to consider strain induced elastic effects on OV formations, other factors, such as polarons in the case of TiO_2, may also have important influences. It is well known that a localized electronic state, the polaron, is very common in TiO_2. Experimentally, small polarons were confirmed in TiO_2 by scanning tunneling microscopy and spectroscopy [18]. Theoretically, the polaronic feature was widely discussed in defective rutile [15], anatase, and other phases of TiO_2 [21]. It is generally argued that the hybrid functionals are necessary for describing localized defect states such as polarons in rutile TiO_2 [13]. For example, the correct polaronic distortion for the electron localization in TiO_2 can only be obtained by the hybrid functional [22]. In this case, the theoretical work [19] using the PW91 functional, which only

considered elastic effects within the continuum elastic model but did not take polaronic effects into account, cannot be sufficient to describe strain effects on OV formations. To clarify the discrepancy between experimental and theoretical findings and fully understand the semiconductor-to-metal transition in bulk rutile TiO_2, both the strain induced elastic and polaronic effects on the formation of OVs should be considered.

In this work we systematically study the strain effects on OVs in bulk rutile TiO_2 using the hybrid functional to take both elastic and polaronic effects into account. We find that strain can have a profound influence on the formation of OVs. Especially, the formation energy of the OV is decreased significantly under biaxial tensile strain and the concentration of conduction electrons can be increased by several orders of magnitude, thus explaining the semiconductor-to-metal transition [20]. Such giant strain effects on OV formations, however, cannot be well described by the continuum elastic model. Under biaxial compressive strain, the model even fails to explain the increase of OV formation energies. Our further investigations show that the failure of the model is attributed to the change of polaronic configurations with strain. Under tensile strain, we find that polarons near OVs are strengthened with large energy gains, thus profoundly reducing the OV formation energies. On the other hand, polarons under compressive strain are suppressed with larger energy cost than elastic energy gain, causing the increase of OV formation energies. This is similar to a hydrogen solution in some bcc metals, where a continuous change of H location with strain was observed [23]. We thus uncover the linkage between the formation of OVs and polarons in rutile TiO_2, and their interplay with strain, which is expected to exist in a wide range of materials.

II. COMPUTATIONAL METHODS

Our calculations are carried out with the Vienna *Ab Initio* Simulation Package (VASP) [24], using the projector augmented-wave method [25] and the Heyd-Scuseria-Ernzerhof functional (HSE06) [26,27]. We have also run tests using 20% Hartree-Fock exchange (see Supplemental Material [28], and also [29–32]) and find that the basic conclusions of our work are unchanged. The energy cutoff is 400 eV and the atoms are relaxed until the forces fall below 0.05 eV/Å. The lattice parameters for the unstrained unit cell are $a = 4.59$ Å and $c = 2.95$ Å, in accordance with the previous theoretical calculations [14,15] and experimental results [33]. For strained unit cells, only the length of the axis perpendicular to the strained plane is allowed to relax. The lattice parameters for the relaxed TiO_2 unit cells are listed in Table I, which are compared with the unstrained ones; positive percent means expansion. OVs in rutile are simulated by removing one oxygen atom from a $2\sqrt{2} \times 2\sqrt{2} \times 4$ supercell, and the single Γ k point is used for the Brillouin zone integration of the supercell. The detailed methods for defect calculations are described in the Supplemental Material [28].

III. RESULTS AND DISCUSSION

A. Formation energy and concentration

Among various types of strain that can be imposed on rutile TiO_2, four cases are considered here: (a) unstrained, (b) at 5% biaxial tensile strain in the (001) plane, (c) at 5% biaxial compressive strain in the (001) plane, and (d) at 4% biaxial tensile strain in the (110) plane. The case of 5% biaxial tensile strain in the (001) plane is adopted here following the experimental setup [20]. Since the (110) surface is the energetically favored one in rutile TiO_2, the strain in the (110) plane is also considered in (d). The case of 4% strain is adopted here because 5% strain is too large in this case and the lattice exhibits obviously broken Ti-O bonds. The strain energies, defined as the energy differences between strained and unstrained rutile per TiO_2 formula, are listed in Table I.

TABLE I. Lattice parameters and strain energies for (a) unstrained rutile, (b) at 5% biaxial tensile strain in the (001) plane, (c) at 5% biaxial compressive strain in the (001) plane, and (d) at 4% biaxial tensile strain in the (110) plane. The lattice parameters in plane l_{in} and out of plane l_{out} are compared with the unstrained ones; positive percent means expansion. The strain energy is defined as the energy difference between strained and unstrained rutile per TiO_2 formula.

Strain type	l_{in}	l_{out}	Strain energy (eV)
a	0	0	0
b	5%	–2.5%	0.16
c	–5%	4.1%	0.20
d	4%	–1.4%	0.17

The calculated formation energies of OVs under different strain are presented in Fig. 1 (The chemical potential of O is limited in the region between −5.1 and 0 eV if single-phase TiO_2 is synthesized. We set it to an intermediate value, −2 eV for (a–c), and −1.5 eV for (d) to keep the formation energies of neutral OVs positive. The detailed values do not influence our conclusions). Comparing the unstrained and strained cases it is obvious that the formation energies of OVs decrease significantly under tensile strain regardless of to which plane the strain is applied. The transition levels become slightly shallower in the strained case. Both the lower formation energies and the shallower transition levels of OVs increase the concentration of electron carriers. Based on the strain energies in Table I and formation energies of OVs in Fig. 1, it can also be concluded that applying tensile strain in (110) needs more energy and is more efficient in introducing OVs. Under compressive strain, to the contrary, the formation energies of OVs increase.

In order to see directly how strain influences the concentration of electron carriers in rutile TiO_2, we make a self-consistent determination of concentrations according to the method generally accepted to estimate defect concentrations [31,32]. Details are found in the Supplemental Material [28]. The concentrations of electron carriers and OVs are presented in Fig. 2. Those in the unstrained case are negligible; the number does not appear in the figure if it is negligible. Under tensile strain the concentrations of electron carriers and OVs show a significant increase, with tensile strain in (110) more effective. This strongly supports the experimental finding of the semiconductor-to-metal transition under tensile strain [20]. Under compressive strain the concentrations are too low to appear in the figure.

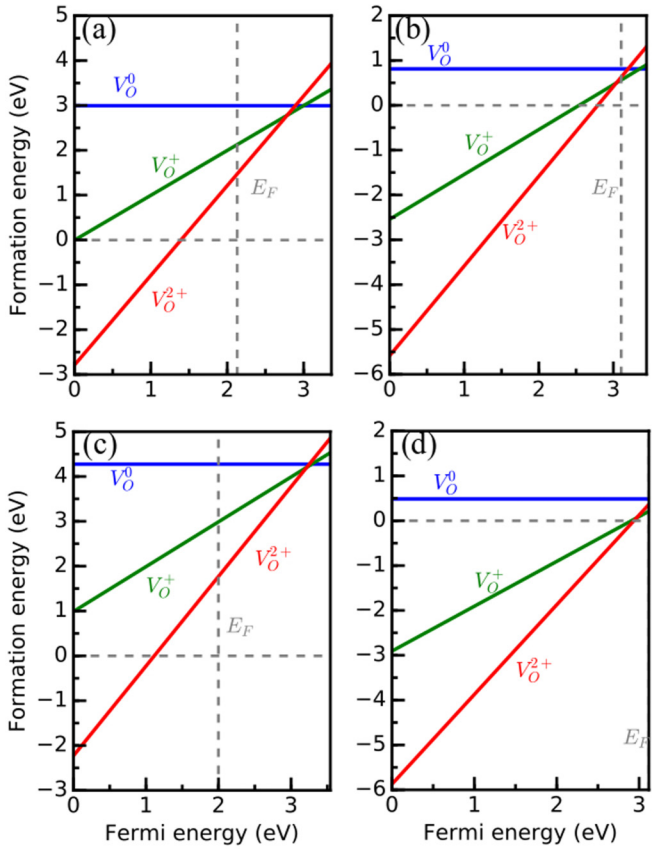

FIG. 1. Calculated formation energies of oxygen vacancies in rutile as a function of the Fermi energy for (a) unstrained rutile, (b) at 5% biaxial tensile strain in the (001) plane, (c) at 5% biaxial compressive strain in the (001) plane, and (d) at 4% biaxial tensile strain in the (110) plane. The equilibrium Fermi energy is determined self-consistently as described in the text.

B. Conflict with the continuum elastic model

To explain the behaviors of rutile TiO_2 under strain, we first resort to the commonly used continuum elastic model. The relative formation energy is defined as the difference of formation energies between OVs in strained and unstrained rutile TiO_2 and given by

$$\begin{aligned}\Delta E_f &= U[\text{host}+\text{defect}] - U[\text{host}] \\ &= \alpha'(V - V[\text{host}+\text{defect}])^2 \\ &\quad - \alpha'(V[\text{host}] - V[\text{host}+\text{defect}])^2 - \alpha(V - V[\text{host}])^2 \\ &= (\alpha' - \alpha)V^2 + 2(\alpha V[\text{host}] \\ &\quad - \alpha' V[\text{host}+\text{defect}])V + C, \end{aligned} \tag{1}$$

where $U[\text{host}]$ and $U[\text{host}+\text{defect}]$ are the strain energy; α and α' are the elastic constants; $V[\text{host}]$ and $V[\text{host}+\text{defect}]$ are the equilibrium volume, for the host lattice and lattice with defects, respectively; and C is some constant. Assuming similar elastic constants for impurity doping, the difference between equilibrium volumes produces a linear change of formation energies with strain [1]. For OVs the decrease in elastic constants explains the parabolic behavior of formation energy versus strain [2]. These two works focus on two different aspects of the continuum elastic model, namely, the equilibrium volumes and the elastic constants.

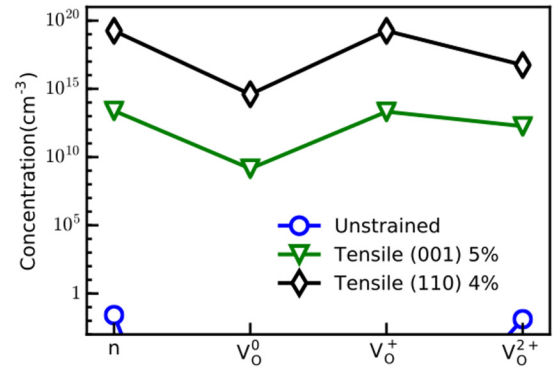

FIG. 2. Estimated concentrations of oxygen vacancies and electrons in conduction bands for (circles) unstrained rutile, (triangles) at 5% biaxial tensile strain in the (001) plane, and (diamonds) at 4% biaxial tensile strain in the (110) plane. Under tensile strain the concentrations show a significant increase while under compressive strain they are too small to appear in the figure.

To fully describe both the expansions in plane and contraction out of plane, a more sophisticated formula for the strain energy U of both the strained host and strained supercell with OVs is adopted here.

$$\begin{aligned} U = \tfrac{1}{2}\big(&C_{11}\varepsilon_1^2 + C_{22}\varepsilon_2^2 + C_{33}\varepsilon_3^2 + C_{23}\varepsilon_2\varepsilon_3 \\ &+ C_{13}\varepsilon_1\varepsilon_3 + C_{12}\varepsilon_1\varepsilon_2\big), \end{aligned} \tag{2}$$

where C and ε are components of the elastic stiffness tensor and strain tensor in Voigt notation, respectively. The relative formation energy is obtained by taking the difference between the strain energies. We have assumed small changes in the equilibrium volumes. The elastic stiffness tensor is calculated using the Perdew-Burke-Ernzerhof (PBE) functional due to the very heavy computational cost if the HSE06 functional is used.

Elastic stiffness tensors for the cells with and without OVs are presented in Table II. As can be seen, most elastic stiffness constants of the supercell with OVs are smaller than those of the pristine host. With OVs in rutile TiO_2, there will be fewer Ti-O bonds; thus it is easier to stretch, and the elastic stiffness constants decrease just like the epitaxial strained $La_{0.5}Sr_{0.5}CoO_{3-\delta}$ film [2]. As rutile TiO_2 is a hard material, large strain can induce a huge elastic effect. Because the formation of OVs decreases the elastic stiffness

TABLE II. Elastic stiffness tensors in Voigt notation for the cells without OV (left) and with OV (right).

Elastic stiffness tensor (GPa)					
C_{ij} $(i,j=1,2,3)$ without OV			C_{ij} $(i,j=1,2,3)$ with OV		
486.2	14.3	172.9	451.3	28.3	163.8
14.3	486.2	172.9	28.3	411.4	143.5
172.9	172.9	486.2	163.8	143.5	475.2
C_{44}	C_{55}	C_{66}	C_{44}	C_{55}	C_{66}
35.3	124.5	124.5	38.4	121.6	123.2

TABLE III. Relative formation energies of neutral oxygen vacancies in rutile for (b) at 5% biaxial tensile strain and (c) at 5% biaxial compressive strain in the (001) plane, predicted by the continuum elastic model E_{model} and by DFT calculations using the HSE06 functional E_{HSE}.

Strain type	(b) Tensile 5%	(c) Compressive 5%
E_{model} (eV)	–1.2	–1.1
E_{HSE} (eV)	–2.2	1.5

significantly, the formation energies of OVs are largely decreased, i.e., by more than 1 eV in Table III, in both tensile and compressive cases according to the continuum elastic model. Our direct DFT calculations, however, do not agree with the model results. Firstly, as seen in Table III, under compressive strain the formation energy calculated by HSE increases rather than decreases as predicted by the model with the strain. Secondly, under tensile strain, although both the model and HSE calculations show the large reduction of OV formation energies compared to the unstrained case, the model-predicted formation energy is much larger than the HSE one. The discrepancy between the continuum elastic model and direct DFT calculations indicates the existence of other factors besides the elastic effect that contribute to defect formation.

C. Polaron formation enhances strain effect

It is well known that small polarons are very common in rutile TiO_2 [18,34] and that they have a profound impact on the material properties such as optical absorptions. Strain naturally connects with polarons since a polaron is a quasiparticle resulting from the electron-phonon interaction. Thus, it is reasonable to take polarons into account when considering strain effects on electronic properties. First, we focus on strain effects on polarons alone, without defects. We discuss the polarons both in unstrained and strained rutile TiO_2 following the method of a previous work [35]. An extra electron is put into the otherwise perfect TiO_2 supercell and two locally stable solutions are found: (1) The lattice does not change and the electron occupies an extended state at the bottom of the conduction band, and (2) the O ions around one Ti ion move outwards slightly and the electron occupies a localized state at this Ti site. The former delocalized solution is obtained directly and the latter polaronic solution requires moving the O ions around one chosen Ti ion outwards before relaxing the structure as proposed by a previous study [36]. Table IV shows the polaron energies, defined as the energy difference between the polaronic and delocalized-electron configurations. A lower energy means that the polaron is more stable. As can be seen, the polaron energy under tensile strain is lower compared with the unstrained case and thus tensile strain benefits polaron formation. In the opposite case, the compressive strain hinders polaron formation, possibly due to the shorter distances between the Ti and O ions and larger Coulomb repulsions between excess electrons and neighboring O ions. In general, the polaron energy change due to strain is small without defects. But, as can be seen in the following, in the presence of OVs, it becomes rather significant.

TABLE IV. Polaron energies, defined as the energy difference between the polaronic and delocalized configurations for (a) unstrained rutile, (b) at 5% biaxial tensile strain in the (001) plane, and (c) at 5% biaxial compressive strain in the (001) plane.

Strain type	(a) Unstrained	(b) Tensile 5%	(c) Compressive 5%
E_p (eV)	–0.14	–0.20	–0.11

Figure 3 shows the spin charge densities of the supercell with neutral OVs. They are caused by the defect states and coincide with the defect charge densities. The orbitals in all strain cases are mainly d_{z^2} and $d_{x^2-y^2}$, but the positions of occupied Ti ions differ. For both the unstrained and tensile strain cases, two neighboring Ti ions far from the OV are occupied with surrounding O ions moving outwards slightly, consisting of a small unit showing polaronic features. The neutral OV donates two electrons and thus there are two such units. For the unstrained case, the charge density distributions of polaronic states obtained in our work are similar with previous work [15]. It is observed experimentally [18] that in rutile, small polarons can stay on many energetically equivalent sites and do not necessarily need to bind with OVs, which is confirmed in our calculated spin charge densities. Comparing the above two cases, we can see that polarons are much strengthened by tensile strain in the presence of OVs, as seen in Figs. 3(a) and 3(b), while larger differences of electron densities are observed under tensile strain. Consequently, the formation energy gain by forming polarons is also significantly increased in the presence of OVs. Comparing the results of the continuum elastic model and HSE calculations in Table III, we estimate this energy gain to be as large as 1 eV. Such a large polaron effect thus much enhances the strain effect on OV formations. For the compressive case, however, the spin charge density as well as polaronic configuration is rather different from the unstrained and tensile strain cases. The electrons now are near the OV, possibly because Ti-O bonds are shorter, and larger Coulomb repulsions between excess electrons and neighboring O ions drive the electrons towards the OVs since there is more room to reduce the Coulomb energy. In this case, each donated electron tends to occupy one Ti ion near the OV and the polaron is largely suppressed, as seen in Fig. 3(c). Consequently, the formation energy gain is much reduced due to the compressive strain, thus causing the increase of OV formation energies. It would be interesting to see in experiments whether under compressive strain, the polarons will move towards the OVs [18].

Through the above analysis, we can conclude that the failure of the continuum elastic model lies in strain changing the polaronic configurations and the occupation of electronic energy levels. The elastic stiffness constants such as the coefficients α and α' in Eq. (1) are the second derivatives of the ground-state energy with respect to the strain, taking the value of the unstrained case. While the polaronic configuration changes with strain, the ground-state wave function no longer varies continuously with strain and thus the derivatives taken at the unstrained point are no longer reliable, resulting in the failure of the continuum elastic model. The strain effect on rutile TiO_2 is reversible as demonstrated in the experiment

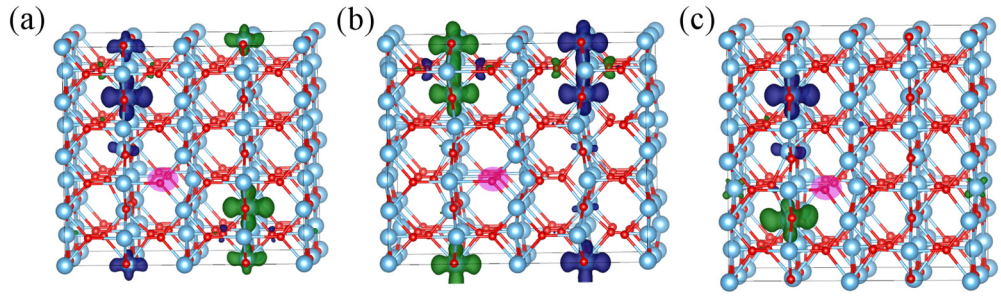

FIG. 3. Spin charge densities of the supercell with neutral oxygen vacancies for (a) unstrained rutile, (b) at 5% biaxial tensile strain in the (001) plane, and (c) at 5% biaxial compressive strain in the (001) plane. Purple transparent areas denote the positions of oxygen vacancies. Light blue atoms are Ti and red atoms are O. Dark blue and green areas denote the spin-up and spin-down charge densities respectively.

[20]. This means that electrons can easily transfer between different Ti sites and the polaronic configuration can change reversibly under strain.

IV. CONCLUSIONS

In conclusion, strain, enhanced by the polaron formation, can induce a giant effect on the formation of OVs in rutile TiO_2. Biaxial tensile strain significantly reduces the formation energies of OVs in rutile TiO_2 and thus the concentrations of electron carriers and OVs increase by several orders of magnitude. Biaxial compressive strain, however, increases the formation energies of OVs, which cannot be understood by the continuum elastic model as strain changes the polaronic configurations and the occupation of electronic energy levels. Polaron formation is enhanced under tensile strain but suppressed under compressive strain. Therefore, under tensile strain the elastic energy reduces the OV formation energy and the favored formations of polarons provide further energy gain, both of which contribute to the giant strain effect. For a hard material, if the formation of vacancies can decrease the elastic stiffness constants considerably, and polaron formation is favored, it is expected that strain can serve as a very effective method to manipulate the defect properties of the material, as demonstrated here in rutile TiO_2.

ACKNOWLEDGMENTS

This work was supported by Science Challenge Project (TZ2018004), National Natural Science Foundation of China (NSFC), National Key Research and Development Program of China (2016YFB0700700), and the Supercomputer Center of Fudan University.

[1] J. Zhu, F. Liu, G. B. Stringfellow, and S.-H. Wei, Phys. Rev. Lett. **105**, 195503 (2010).
[2] W. Donner, C. Chen, M. Liu, A. J. Jacobson, Y.-L. Lee, M. Gadre, and D. Morgan, Chem. Mater. **23**, 984 (2011).
[3] J. R. Petrie, H. Jeen, S. C. Barron, T. L. Meyer, and H. N. Lee, J. Am. Chem. Soc. **138**, 7252 (2016).
[4] J. R. Petrie, C. Mitra, H. Jeen, W. S. Choi, T. L. Meyer, F. A. Reboredo, J. W. Freeland, G. Eres, and H. N. Lee, Adv. Funct. Mater. **26**, 1564 (2016).
[5] Z. T. Wang, S. Chen, X. M. Duan, S.-H. Wei, D. Y. Sun, and X. G. Gong, J. Phys.: Condens. Matter **24**, 215801 (2012).
[6] Z.-W. Wang, D.-J. Shu, M. Wang, and N.-B. Ming, Surf. Sci. **606**, 186 (2012).
[7] Z. Wang, S. Chen, X. Duan, D. Sun, and X. Gong, J. Phys. Soc. Jpn. **81**, 074712 (2012).
[8] A. Fujishima and K. Honda, Nature **238**, 37 (1972).
[9] M. Valden, X. Lai, and D. W. Goodman, Science **281**, 1647 (1998).
[10] F. D. Brandao, M. V. B. Pinheiro, G. M. Ribeiro, G. Medeiros-Ribeiro, and K. Krambrock, Phys. Rev. B **80**, 235204 (2009).
[11] C. M. Yim, C. L. Pang, and G. Thornton, Phys. Rev. Lett. **104**, 036806 (2010).
[12] A. T. Brant, E. M. Golden, N. C. Giles, S. Yang, M. A. R. Sarker, S. Watauchi, M. Nagao, I. Tanaka, D. A. Tryk, A. Manivannan, and L. E. Halliburton, Phys. Rev. B **89**, 115206 (2014).
[13] C. Di Valentin, G. Pacchioni, and A. Selloni, Phys. Rev. Lett. **97**, 166803 (2006).
[14] A. Janotti, J. B. Varley, P. Rinke, N. Umezawa, G. Kresse, and C. G. Van de Walle, Phys. Rev. B **81**, 085212 (2010).
[15] P. Deak, B. Aradi, and T. Frauenheim, Phys. Rev. B **86**, 195206 (2012).
[16] S. Wendt, P. T. Sprunger, E. Lira, G. K. H. Madsen, Z. Li, J. O. Hansen, J. Matthiesen, A. Blekinge-Rasmussen, E. Laegsgaard, B. Hammer, and F. Besenbacher, Science **320**, 1755 (2008).
[17] P. Deak, B. Aradi, and T. Frauenheim, Phys. Rev. B **92**, 045204 (2015).
[18] M. Setvin, C. Franchini, X. F. Hao, M. Schmid, A. Janotti, M. Kaltak, C. G. Van de Walle, G. Kresse, and U. Diebold, Phys. Rev. Lett. **113**, 086402 (2014).
[19] D.-J. Shu, S.-T. Ge, M. Wang, and N.-B. Ming, Phys. Rev. Lett. **101**, 116102 (2008).
[20] E. E. Benson, E. M. Miller, S. U. Nanayakkara, D. Svedruzic, S. Ferrere, N. R. Neale, J. van de Lagemaat, and B. A. Gregg, Chem. Mater. **29**, 2173 (2017).
[21] F. De Angelis, C. Di Valentin, S. Fantacci, A. Vittadini, and A. Selloni, Chem. Rev. **114**, 9708 (2014).

[22] C. Di Valentin, E. Finazzi, G. Pacchioni, A. Selloni, S. Livraghi, M. C. Paganini, and E. Giamello, Chem. Phys. **339**, 44 (2007).
[23] H. B. Zhou, S. Jin, Y. Zhang, G. H. Lu, and F. Liu, Phys. Rev. Lett. **109**, 135502 (2012).
[24] G. Kresse and J. Furthmüller, Phys. Rev. B **54**, 11169 (1996).
[25] G. Kresse and D. Joubert, Phys. Rev. B **59**, 1758 (1999).
[26] J. Heyd, G. E. Scuseria, and M. Ernzerhof, J. Chem. Phys. **118**, 8207 (2003).
[27] A. V. Krukau, O. A. Vydrov, A. F. Izmaylov, and G. E. Scuseria, J. Chem. Phys. **125**, 224106 (2006).
[28] See Supplemental Material at http://link.aps.org/supplemental/10.1103/PhysRevB.99.014113 for methods of defect calculations and concentration estimations and test results changing the proportion of Hartree-Fock exchange.
[29] P. Deak, B. Aradi, and T. Frauenheim, Phys. Rev. B **83**, 155207 (2011).
[30] A. Malashevich, M. Jain, and S. G. Louie, Phys. Rev. B **89**, 075205 (2014).
[31] C. Persson, Y. J. Zhao, S. Lany, and A. Zunger, Phys. Rev. B **72**, 035211 (2005).
[32] Y. Kumagai, M. Choi, Y. Nose, and F. Oba, Phys. Rev. B **90**, 125202 (2014).
[33] F. A. Grant, Rev. Mod. Phys. **31**, 646 (1959).
[34] V. N. Bogomolov and D. N. Mirlin, Phys. Status Solidi B **27**, 443 (1968).
[35] A. Janotti, C. Franchini, J. B. Varley, G. Kresse, and C. G. Van de Walle, Phys. Status Solidi RRL **7**, 199 (2013).
[36] T. Shibuya, K. Yasuoka, S. Mirbt, and B. Sanyal, J. Phys.: Condens. Matter **24**, 435504 (2012).